

Linearity of amplitude and phase in tapping-mode atomic force microscopy

M. V. Salapaka

Electrical Engineering Department, Iowa State University, Ames, Iowa 50011

D. J. Chen

Electrical Engineering Department, Iowa State University, Ames, Iowa 50011

J. P. Cleveland

Digital Instruments, Santa Barbara, California 93117

(Received 8 April 1999; revised manuscript received 30 July 1999)

In this article tapping-mode atomic force microscope dynamics is studied. The existence of a periodic orbit at the forcing frequency is shown under unrestrictive conditions. The dynamics is further analyzed using the impact model for the tip-sample interaction and a spring-mass-damper model of the cantilever. Stability of the periodic orbit is established. Closed-form expressions for various variables important in tapping-mode imaging are obtained. The linear relationship of the amplitude and the sine of the phase of the first harmonic of the periodic orbit with respect to cantilever-sample offset is shown. The study reinforces gentleness of the tapping-mode on the sample. Experimental results are in excellent qualitative agreement with the theoretical predictions. The linear relationship of the sine of the phase and the amplitude can be used to infer sample properties. The comparison between the theory and the experiments indicates essential features that are needed in a more refined model.

I. INTRODUCTION

The atomic force microscope (AFM) has revolutionized imaging in the past decade and has contributed significantly to the physical and biological sciences (see Ref. 1). Since its invention in 1986 (see Ref. 2), a wide range of imaging modes of operation have emerged. These were primarily motivated by the drawbacks of the original contact-mode imaging.

Arguably, tapping mode is the most widely used mode in AFM imaging that overcomes most of the difficulties present in the contact-mode operation. In this mode the cantilever base is subjected to sinusoidal forcing at the first resonance frequency of the cantilever, inducing a periodic oscillation of the cantilever. The sample properties are inferred by analyzing the changes in the cantilever's oscillations due to the interaction between the sample and the tip that is mounted on the free end of the cantilever.

The interaction between the tip and the sample is highly nonlinear. Unlike contact mode, in tapping mode the tip moves through the whole range of the tip-sample potential. Thus, a linear model of the interaction is inadequate (see Ref. 3). Furthermore, the existence of chaotic behavior is established for models of such an interaction (see Refs. 4 and 5). Experimental evidence for such behavior is also present (see Ref. 6).

Under normal operating conditions, in spite of the complex nature of the nonlinear interaction between the tip and the sample, the cantilever is found to evolve into a stable periodic orbit with a period equal to the period of the forcing. Experimental data also reveal that when the offset between the sample and the cantilever is relatively large, the periodic orbit is nearly sinusoidal (see Ref. 7).

Numerical simulations of complex models of the tip-

sample interaction have reproduced the experimental observations (see Refs. 3, 8–11). However, there is a lack of theoretical analysis on why the cantilever behaves in such a manner. To bridge this gap we first establish the existence of a periodic orbit with unrestrictive assumptions on the dynamics.

One of the simplest tip-sample interactions that can be imagined is an impact interaction where the sample behaves as a reflecting surface. The energy losses in this interaction are characterized by a coefficient of restitution λ . Using this model, analytical expressions for parameters important for imaging are obtained. In particular, expressions for the periodic orbit, the velocity with which the cantilever tip hits the sample, and amplitude and phase of the first harmonic of the periodic orbit are derived. Given that the orbit is nearly sinusoidal, only three variables are required to describe the periodic orbit; the dc offset, the amplitude and phase (with respect to the forcing) of the sine wave. A way to obtain these variables is given.

For tapping-mode AFM's operating in air, the air damping is small. By expanding the analytical expressions in terms of the damping ratio and ignoring the higher-order terms, useful relationships between various parameters are obtained. Such a study predicts that the amplitude and the sine of the phase of the first harmonic of the periodic oscillation of the cantilever vary linearly with respect to the offset between the cantilever and the sample. Such relationships offer new ways of inferring sample properties.

Experiments conducted have corroborated the theoretical studies. Such a comparison has confirmed the linearity of the amplitude and the sine of the phase of the first harmonic of the cantilever's periodic oscillations. The analysis of the discrepancy between the experimentally evaluated energy lost to the sample and the theoretically predicted values pro-

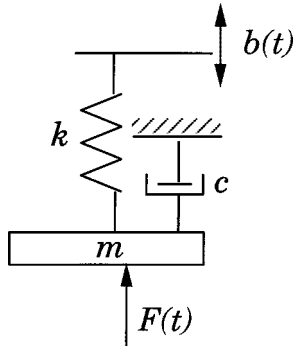


FIG. 1. The cantilever is modeled by a spring and a mass. The base of the cantilever is subjected to a sinusoidal motion given by $b(t)$. The air damping is proportional to the velocity of the mass with respect to an inertial frame.

vides significant insights into the tapping-mode dynamics and indicates essential features that need to be incorporated in a more refined model.

II. MODELING

In the tapping-mode operation of an AFM a dither piezo attached to the substrate that forms the support of the cantilever is forced sinusoidally (see Fig. 5 below). In most applications the first-mode approximation for the cantilever vibration is adequate for explaining the experimentally observed characteristics. In this article we will assume the one-mode approximation and hence, the dynamics of Fig. 1. In this case, the dynamical equation for the displacement of the cantilever is given by

$$m\ddot{p} + c\dot{p} + kp = kb(t) + F(t), \quad (1)$$

where m , c , and k are the effective mass, the viscous damping coefficient, and the spring constant, respectively, of the free cantilever. F is the force on the cantilever due to the sample and b describes the displacement of the base of the cantilever. The nominal position of the cantilever tip is defined to be the equilibrium position the cantilever tip takes when there are no forces due to the sample ($F=0$) and when the cantilever-base is stationary ($b=0$). $p(t)$ is the instantaneous position of the cantilever tip measured from its nominal position. p is considered positive when the cantilever-tip position is farther away from the sample when compared to the nominal position of the cantilever tip.

Equation (1) can be recast as

$$\ddot{p} + 2\xi\omega\dot{p} + \omega^2 p + h(p, \dot{p}, l) = g(t), \quad (2)$$

where $\omega = \sqrt{k/m}$, $2\xi\omega = c/m$, $g(t) = [kb(t)]/m$, and $h = -(F/m)$. The parameter l characterizes the separation between the tip of the cantilever and the sample when the tip of the cantilever is at the nominal position. We will also use the term *cantilever-sample separation* to mean l . Note that this phrase should not be confused with the instantaneous separation between the tip and the sample.

The sample force per unit mass is assumed to be dependent on the position of the cantilever, the velocity of the cantilever, and the parameter l . In most tapping-mode applications $b(t)$ is a sinusoidal function. Consequently, we assume that $g(t) = -\gamma \cos \omega t$. Further, to conform with most

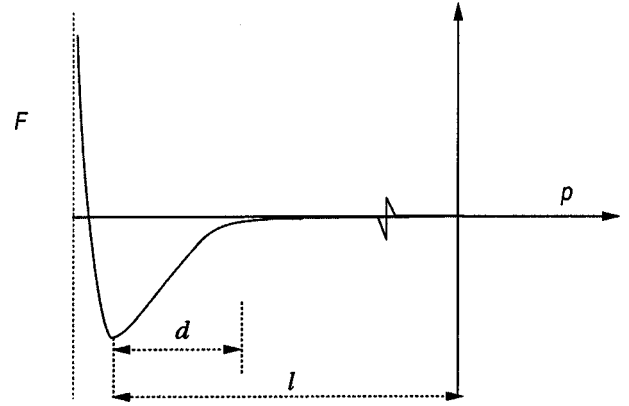


FIG. 2. Sketch of a typical tip-sample force. The force on the cantilever due to the sample is given by F . The sample has a long-range attractive force that can be neglected after a separation ($l-d$). For short separations the forces are strongly repulsive. d is the difference in the separations at which the repulsive and the attractive forces become significant.

applications of the tapping mode it is assumed that ω is equal to the first natural frequency of the free cantilever.

Experimental data has indicated that a force curve of the form shown in Fig. 2 well characterizes the force on the cantilever due to the sample. It indicates long-range attractive forces and short-range strong repulsive forces. According to this model, the sample has negligible influence on the cantilever when the separation between the tip and the sample is larger than $(l-d)$ [that is, $p \geq -(l-d)$]. We will use this observation in the next section to establish the existence of the periodic orbit with unrestrictive assumptions on the tapping-mode operation.

In most tapping-mode applications the cantilever-sample separation is large when compared to the length scale of interaction ($l \gg d$) (see Fig. 2). Also, the fraction of the time that the cantilever tip spends inside the sample [$p < -(l-d)$] is small compared to the fraction of the time it spends in air [$p \geq -(l-d)$]. The small amount of time spent inside the sample motivates the impact model of the tip-sample interaction, where we assume that the sample can be modeled as a hard wall. In this model, whenever the mass m hits the wall with a velocity v it reflects off the wall with a velocity $-\lambda v$ (see Fig. 3). λ is often called the coefficient of restitution.

Another motivating factor in studying the impact model is that this model is tractable and explicit analytical expressions for various parameters important for imaging can be obtained (as will be seen). Such expressions seem unlikely for a more detailed model of the tip-sample interaction.

III. ANALYSIS

A. Existence

It is experimentally observed that for a wide variety of operating conditions the tapping cantilever settles into a periodic orbit with the same period as that of the forcing. Even though the tapping mode has been used and researched extensively there is a lack of analysis on why the cantilever settles into such a periodic orbit. In particular the existence of the periodic orbit has not received attention.

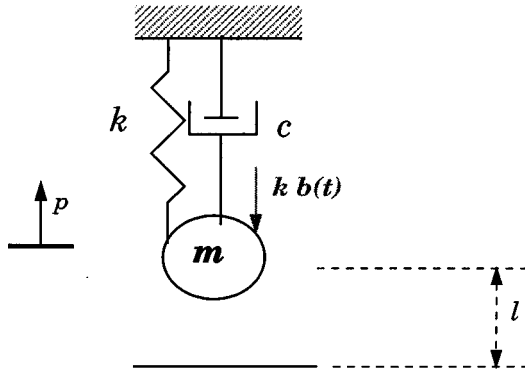


FIG. 3. The figure depicts the impact model of the tip-sample interaction. In this model the sample is modeled as a hard wall. The mass m reflects off the sample with a velocity $-\lambda v$ when the mass displacement equals $-l$ and the velocity with which the mass hits the sample is given by v . Note that the displacement is positive upwards; that is, it is positive when the mass is farther away from the sample when compared to the nominal position.

The cantilever dynamics given in Eq. (1) can be transformed into a first-order state equation;

$$\begin{aligned} \begin{pmatrix} \dot{x}_1 \\ \dot{x}_2 \end{pmatrix} &= \begin{pmatrix} x_2 \\ -\omega^2 x_1 - 2\xi\omega x_2 - h(x_1, x_2) \end{pmatrix} + \begin{pmatrix} 0 \\ 1 \end{pmatrix} g(t) \\ &=: f_1(x) + f_2(x)g(t), \end{aligned} \quad (3)$$

where $x_1 = p$ is the position of the cantilever with respect to an inertial frame, and $x_2 = \dot{p}$. Note that if the sample is far away from the tip, then the influence of the sample on the cantilever dynamics can be neglected and the cantilever behaves as a damped linear oscillator. More specifically, we assume that $h=0$ if $x_1 \geq -(l-d)$. Note that estimates of $(l-d)$ and l can be obtained from experimental data.

We will denote the period of the sinusoidal forcing $g(t)$ by T . We first argue that it is not possible for any orbit, $p(t)$, of Eq. (3) to be periodic with period less than T . Suppose $\phi(t)$ is a solution to Eq. (3) with $\phi(t) = \phi(t+T')$ for all t with $T' < T$. Then it follows that $\dot{\phi}(t) = \dot{\phi}(t+T')$ for all t , which implies that $f_1[\phi(t)] + f_2[\phi(t)]g(t) = f_1[\phi(t+T')] + f_2[\phi(t+T')]g(t+T')$, for all t . As $\phi(t) = \phi(t+T')$, $f_1[\phi(t)] = f_1[\phi(t+T')]$, and because $f_2[\phi(t)] = (0, 1)'$ it follows that $g(t) = g(t+T')$ for all t . This is a contradiction to the fact that g is sinusoidal with period T . Thus, if we establish the existence of any T periodic orbit then we have established the existence of a periodic orbit with least period T (for example a $T/2$ periodic orbit is also T periodic orbit, but, is ruled out by the above arguments).

For establishing the existence of a T periodic orbit we use a result by Poincaré that addresses the existence of a periodic solution for a dynamical system, $\dot{x} = f(x, t)$, where $f(x, t)$ [for Eq. (3), $f(x, t) = f_1(x) + f_2(x)g(t)$] is a T periodic function. This result says that if there is a suitable set D in the phase space (x_1, x_2) in R^2 , which has the property that any trajectory $x[t, 0, x(0)]$, starting at time 0 and state $x(0)$ in D remains in D for all $t \geq 0$ (such a set is said to be positively-invariant under the given dynamics), then there is a T periodic solution of $\dot{x} = f(x, t)$ in D (see Ref. 12). Such a set D is constructed for the tapping-mode dynamics in the Appendix. As explained in the Appendix, the assumptions made in the

construction of such a set are unrestrictive. For the remainder of the work we will assume that there exists a T periodic orbit for the tapping-mode dynamics.

B. Impact model

In this section we model the sample by a hard wall. Consider the mass m in Fig. 3, which hits the sample modeled as a hard wall for the n th time with a velocity \dot{p}_n at time instant t_n . The mass m reflects off the wall with a velocity $-\lambda \dot{p}_n$ instantaneously. For the purposes of intuition, a common macroscopic system that is modeled by this dynamics is a rubber ball bouncing off a hard floor. The motion of the mass is governed by Eq. (4) given by

$$\begin{pmatrix} \dot{x}_1 \\ \dot{x}_2 \end{pmatrix} = \begin{pmatrix} x_2 \\ -\omega^2 x_1 - 2\xi\omega x_2 \end{pmatrix} + \begin{pmatrix} 0 \\ 1 \end{pmatrix} g(t), \quad (4)$$

with initial conditions at time t_n given by $(-l, -\lambda \dot{p}_n)$ till a time t_{n+1} when the mass hits the sample again. The solution of Eq. (4) with initial conditions at time instant t_0 given by $p(t_0) = -l$ and $\dot{p}(t_0) = \dot{p}_0$ is solved to be

$$\begin{aligned} p(t) &= -l_0 \sin \omega t + e^{-\xi\omega(t-t_0)} \{C_1 \cos \bar{\omega}(t-t_0) \\ &\quad + C_2 \sin \bar{\omega}(t-t_0)\}, \end{aligned} \quad (5)$$

where

$$C_1 = -l + l_0 \sin \omega t_0,$$

$$C_2 = \frac{1}{\bar{\omega}} \{ \xi\omega(-l + l_0 \sin \omega t_0) + \dot{p}_0 + l_0\omega \cos \omega t_0 \},$$

$$l_0 = \frac{\gamma}{2\xi\omega^2} \quad \text{and} \quad \bar{\omega} = \omega\sqrt{1-\xi^2}.$$

l_0 is the amplitude of the free cantilever (that is, the amplitude at steady state with no sample present). Differentiating Eq. (5) with respect to t we obtain,

$$\begin{aligned} \dot{p}(t) &= -l_0\omega \cos \omega t + e^{-\xi\omega(t-t_0)} \\ &\quad \times \{C_3 \cos \bar{\omega}(t-t_0) + C_4 \sin \bar{\omega}(t-t_0)\}, \end{aligned} \quad (6)$$

where

$$C_3 = (\dot{p}_0 + l_0\omega \cos \omega t_0),$$

$$C_4 = -\frac{\omega}{\bar{\omega}} \{ \omega(-l + l_0 \sin \omega t_0) + \xi(\dot{p}_0 + l_0\omega \cos \omega t_0) \}.$$

On the T periodic orbit (whose existence was established in the previous section), $t_{n+1} = T + t_n$ and $\dot{p}_{n+1} = \dot{p}_n$. Thus on the periodic orbit, if the time immediately after impact is denoted by t_0 then taking advantage of the instantaneous nature of the impact, we have that

$$p(t_0 + T) = -l \quad (7)$$

and

$$\dot{p}(t_0 + T) = -\frac{1}{\lambda} \dot{p}(t_0). \quad (8)$$

Upon substituting Eqs. (5) and (6) into Eqs. (7) and (8) we observe that $\cos \omega t_0$, $\sin \omega t_0$, \dot{p}_0 , and l appear linearly in Eqs. (7) and (8). By eliminating \dot{p}_0 from Eqs. (7) and (8) we obtain

$$X \cos \omega t_0 + Y \sin \omega t_0 = D, \quad (9)$$

where X, Y, D are provided in the Appendix.

From Eq. (9) we have that

$$\sin(\theta + \omega t_0) = \frac{D}{\sqrt{X^2 + Y^2}} = \frac{l}{l_0} \left(\frac{Y}{\sqrt{X^2 + Y^2}} \right). \quad (10)$$

By expanding the right-hand side in powers of the parameter ξ we can show that

$$\sin(\theta + \omega t_0) = \frac{l}{l_0} [1 + O(\xi^2)], \quad (11)$$

where

$$\sin(\theta) = \frac{X}{\sqrt{X^2 + Y^2}} = \frac{\xi}{2} + O(\xi^2). \quad (12)$$

Thus it follows that

$$\sin \omega t_0 = \frac{l}{l_0} [1 + O(\xi^2)] + O(\xi). \quad (13)$$

By eliminating $\sin \omega t_0$ from Eqs. (7) and (8) we obtain

$$\dot{p}_0 = -M l_0 \omega \cos \omega t_0, \quad (14)$$

where

$$M = -\lambda \frac{1 + e^{-4\xi\pi} - 2e^{-2\xi\pi} \cos(2\pi\sqrt{1-\xi^2})}{1 - \lambda e^{-4\xi\pi} + (\lambda - 1)e^{-2\xi\pi} \cos(2\pi\sqrt{1-\xi^2}) - (\lambda + 1)e^{-2\xi\pi} \sin(2\pi\sqrt{1-\xi^2})} = -\frac{2\pi\xi\lambda}{1+\lambda} + O(\xi^2). \quad (15)$$

Thus we have that the velocity of impact on the periodic orbit is given by

$$\begin{aligned} \dot{p}_\perp &:= \dot{p} \left(t_0 + \frac{2\pi}{\omega} \right) = + \frac{1}{\lambda} M l_0 \omega \cos \omega t_0 \\ &= - \left(\frac{2\pi\xi}{1+\lambda} + O(\xi^2) \right) l_0 \omega \cos \omega t_0. \end{aligned} \quad (16)$$

Thus the periodic orbit is defined by Eq. (5) with t_0 given by Eq. (11), $p_0 = -l$ and \dot{p}_0 given by Eq. (14). Thus we have an explicit solution for the periodic orbit in the impact case.

Note that we have provided expansions of the various quantities derived, in terms of the parameter ξ . For tapping-mode AFM's that operate in air, ξ is small. Thus we can ignore the higher-order terms of ξ to assess the behavior of the dominant terms.

The velocity of impact on the periodic orbit [given in Eq. (16)] is proportional to ξ . Thus the velocity of impact is small in general and is particularly small if the cantilever-sample separation l is large [note that $\cos \omega t_0 \approx 1/l_0 \sqrt{l_0^2 - l^2}$ in Eq. (16)]. It is also evident that the impact velocity varies by only a factor of 2 and remains small over the whole range of the parameter λ ($0 \leq \lambda \leq 1$), where no energy is lost upon impact if $\lambda = 1$, and all the energy is lost upon impact if $\lambda = 0$. It needs to be stressed that the analysis here indicates that irrespective of the sample (characterized by λ) the state of the system evolves into a periodic orbit that is gentle on the sample provided that the air damping of the cantilever is small. This explains the experimentally observed gentleness of the tapping-mode operation on the sample. In Fig. 4, a plot of the impact velocity versus the tip-sample separation l for various values of λ is presented. As can be clearly seen, the velocity at impact increases with decreasing tip-sample separation and with decreasing λ .

Based on the impact velocity given in Eq. (16) we can evaluate the energy lost upon impact to be

$$E_l = 2\pi^2 k \xi^2 (l_0^2 - l^2) \frac{1-\lambda}{1+\lambda}. \quad (17)$$

Thus the energy lost due to impact is proportional to ξ^2 . Note that when $\lambda = 0$ (inelastic impact) the energy loss during impact is $2\pi^2 k \xi^2 (l_0^2 - l^2)$. We will elucidate more on the energy lost in the next section.

We now study the stability of the periodic orbit using another result by Poincaré (see Ref. 12). Suppose the canti-

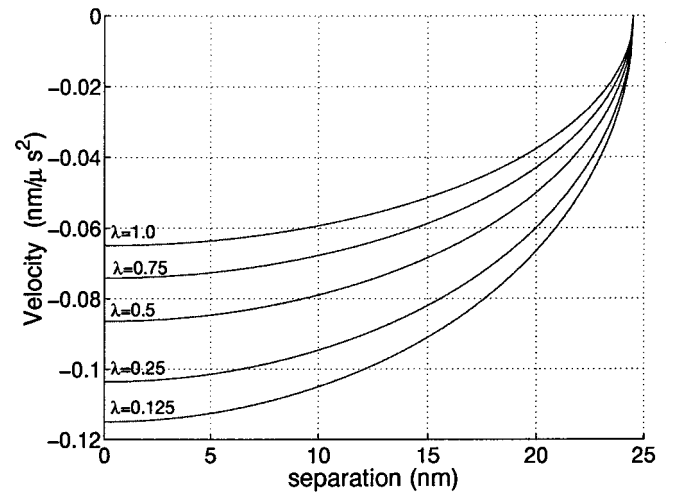


FIG. 4. This figure shows a plot of the impact velocity versus the cantilever-sample separation l for various values of λ . It can be seen that as the factor λ is decreased the impact velocity increases. However, over the whole range of the possible values of λ the impact velocity is small and varies only by a factor of 2.

lever tip is at a certain initial condition that is close to the periodic orbit established earlier. With this initial condition let the map from the n th impact time and the n th impact velocity to the $(n+1)$ th impact time and the $(n+1)$ th impact velocity for the orbit resulting from the given initial condition be given by P . Thus,

$$\begin{pmatrix} \dot{p}_{n+1} \\ t_{n+1} \end{pmatrix} = \begin{pmatrix} P_1(\dot{p}_n, t_n) \\ P_2(\dot{p}_n, t_n) \end{pmatrix} =: P(\dot{p}_n, t_n).$$

Poincaré's result says that the periodic orbit is stable if all the eigenvalues of the Jacobian of the map P on the periodic orbit have modulus less than one. The Jacobian is given by

$$DP = \begin{pmatrix} \frac{\partial P_1}{\partial \dot{p}_n} & \frac{\partial P_1}{\partial t_n} \\ \frac{\partial P_2}{\partial \dot{p}_n} & \frac{\partial P_2}{\partial t_n} \end{pmatrix}.$$

Note that we have derived the analytical expression of the periodic orbit. However, we have not derived the form of the orbit resulting from initial condition not on the periodic orbit. This task is impossible due to the transcendental form of the equations involved. However, the elements of DP can be obtained by implicit differentiation that is provided in the Appendix. In the limit $\xi \rightarrow 0$ the eigenvalue of the Jacobian is given by $-\lambda e^{-2\xi\pi}$. Thus the periodic orbit will be stable if $\lambda < 1$.

C. Relation of the amplitude and phase of the first harmonic with respect to the cantilever-sample separation

Tapping-mode AFM's provide the amplitude and phase of the first harmonic of the periodic orbit as measured quantities. These quantities can be used for imaging sample properties if their relationships to the properties are established. In a recent result, based on the assumption that the steady-state cantilever oscillations can be approximated by a pure sinusoid, a method has been devised for imaging energy losses to the sample using the amplitude and phase of the sinusoid (see Ref. 7). With this motivation we study the first harmonic of the periodic orbit resulting from the impact model of the tip-sample interaction.

Note that we have obtained an analytical expression for the periodic orbit in the impact case in the previous subsection. Thus we can obtain the Fourier coefficient of the first-harmonic component by performing the integral

$$\begin{aligned} Y_1 &= \frac{\omega}{2\pi} \int_{t_0}^{(2\pi/\omega)+t_0} p(t) e^{-j\omega t} dt \\ &= \frac{\omega}{2\pi} e^{-j\omega t_0} \int_{t_0}^{(2\pi/\omega)+t_0} p(t) e^{-j\omega(t-t_0)} dt, \end{aligned}$$

where $p(t)$ is given by Eq. (5). We can evaluate the integral to be

$$\begin{aligned} Y_1 &= \left[-\frac{l_0}{2} \sin \omega t_0 + j \left(\frac{1}{2} + \frac{(1+\lambda)M}{4\pi\xi\lambda} \right) l_0 \cos \omega t_0 \right] e^{-j\omega t_0} \\ &= \left(-\frac{1}{2} l [1 + O(\xi^2)] + j O(\xi) \right) e^{-j\omega t_0}. \end{aligned} \quad (18)$$

Note that the amplitude A of the first harmonic is given by

$$A := 2|Y_1| = l [1 + O(\xi^2)] + O(\xi^2). \quad (19)$$

Thus the analysis of the impact model predicts that the cantilever-sample separation l can be accurately predicted by the amplitude A of the first harmonic of the periodic orbit.

This conclusion might seem trivial as the cantilever-tip displacement towards the sample cannot be more than the distance between its nominal position and the sample modeled as a hard wall (otherwise the cantilever tip would penetrate the hard wall). Thus if the sample moves by Δl the maximum displacement of the cantilever towards the sample also has to change by Δl . Thus the linear relationship between l and the maximum displacement of the cantilever tip towards the sample can be argued in this way. However, Eq. (19) predicts a linear relationship between the amplitude of the *first harmonic* of the periodic orbit and l . If the wall is found at a distance $-w$, what is surprising and nonintuitive is that the tip never goes a distance w above the cantilever's rest position. That is, there is a physical reason to expect the oscillation to be bounded by $-w$, but no reason to expect it to be bounded by $+w$. The fact that the orbit stays symmetric means that the average deflection of the cantilever tip is always small and all the surface information is carried (linearly) in the amplitude. Note that the periodic orbit whose existence was established earlier could be nonsinusoidal and thus could have higher harmonics. Indeed the spectral analysis of experimental data reveals such harmonics. The important insight offered by Eq. (19) is that the higher harmonics can be safely neglected and thus the periodic oscillation of the cantilever tip can be approximated by a sinusoid. This result also gains significance because it is experimentally convenient to obtain the amplitude and the phase of the first harmonic of the periodic orbit rather than obtaining the complete time history or even the data on higher harmonics. The hardware needed to extract the amplitude and phase of the first harmonic is less involved and costs less because of the lower bandwidths of the equipment needed. Note that the information on the dc offset (the average deflection of the cantilever tip) is lost when evaluating the first harmonic of the periodic orbit. However, this can be evaluated by finding the constant term in the Fourier expansion of the periodic solution.

This implies that amplitude can be effectively employed to image the topography of the sample, particularly when the damping is small. In a way, the amplitude is used to image the topography in a standard tapping AFM because the z feedback loop (see Fig. 5) keeps the amplitude constant. However, this would still work even if the amplitude versus l were nonlinear. The result here is even stronger. If no feedback was used the amplitude signal would accurately measure sample topography. To employ this practically would require much larger amplitudes than are commonly used.

The phase of the first harmonic with respect to the forcing is given by $\phi = \arg(Y_1) - \pi = -\omega t_0 + O(\xi)$. Therefore we have

$$\sin \phi = -\sin \omega t_0 + O(\xi) = -\frac{l}{l_0} [1 + O(\xi^2)] + O(\xi). \quad (20)$$

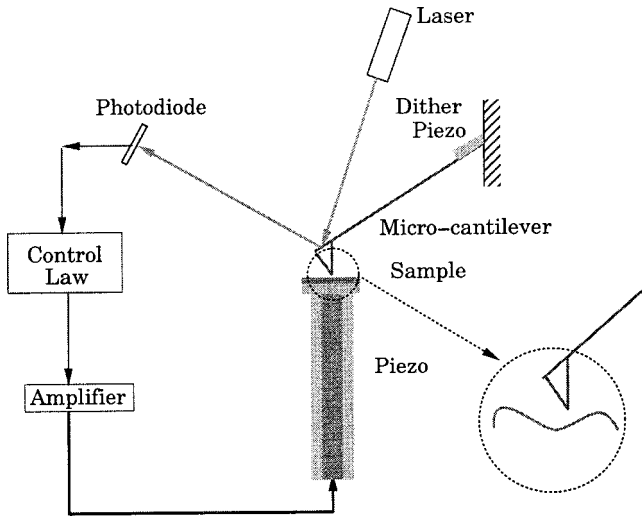


FIG. 5. This figure describes the experimental setup used. The sample is positioned using a piezotube. The cantilever is oscillated using a sinusoidal voltage applied to the dither piezo. The displacement of the cantilever is recorded by a laser that reflects off the cantilever surface and is incident into a split photodiode sensor.

The relationship above says that the sine of the phase of the first harmonic (the phase with respect to the forcing) varies linearly with respect to the cantilever-sample separation. Traditionally, most researchers have focused on the plots of the phase versus the cantilever-sample separation. However, the analysis presented leads to an important observation; studying the sine of the phase versus cantilever-sample separation curve can be more illuminating than phase versus cantilever-sample separation curve due to the linear nature of the former.

Recently in Ref. 7, a method was devised to estimate the power dissipated in the tapping-mode AFM. This was achieved by equating the energy input from the forcing and the energy lost to the damping and the sample. The assumption made is that the periodic orbit is sinusoidal. Using this method it is found that the power lost due to the interaction with sample is given by

$$\xi k A^2 \omega \left(\frac{l_0}{A} \sin \phi + 1 \right). \quad (21)$$

Note that the prefactor in Eq. (21) is the power loss due to air damping. Since the impact model predicts that the $A \approx l$ and that $\sin \phi \approx -(l/l_0)$, the loss of energy due to the tip-sample interaction is always small compared to air-damping losses. This is also evident from Eq. (17). Note that Eqs. (17) and (21) can be equated to evaluate the coefficient λ . This means that images of amplitude and phase could be used to make images of λ . However, as will be seen in the next section, the losses seen experimentally for most samples are much larger than the limit $2\pi^2 k \xi^2 (l_0^2 - l^2)$.

IV. EXPERIMENTAL METHODS AND DISCUSSION

An atomic force microscope (MultiMode, Digital Instruments, Santa Barbara, CA) was operated in tapping mode (see Ref. 13). The experimental setup is described by Fig. 5. The sample is positioned vertically by a piezo ceramic tube.

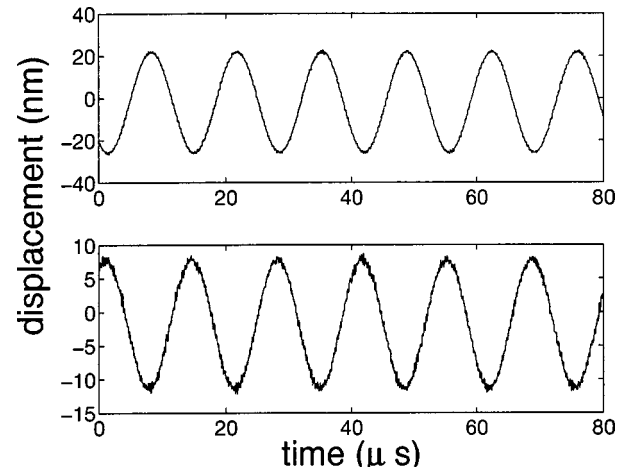


FIG. 6. This figure shows the plots of the tip deflection for two different values of cantilever-sample separation l . The plot on the top shows the time plot of the tip deflection for a large cantilever-sample separation whereas the plot below shows the time plot of the tip deflection for a smaller value of the cantilever-sample separation. It is evident that in both cases the cantilever tip is on a periodic orbit. This is also confirmed by a spectral analysis of the time plots. It can be seen that the cantilever-tip oscillations are almost sinusoidal. The spectral analysis also shows that when the cantilever-sample separation is small the orbit deviates more from a sinusoidal orbit.

The position of the base of the cantilever can be controlled by applying a voltage to the dither piezo. The displacement of the cantilever is recorded by using a laser that reflects off the cantilever surface and which is incident on a split photodiode. A silicon cantilever of length $225 \mu\text{m}$ was used. The model parameters were evaluated by analyzing the cantilever response to thermal noise in similar ways to the those suggested in Refs. 14 and 15. The quality factor Q of the cantilever was evaluated to be 130, (Q is given by $\sqrt{km/c}$). Thus, we have $\xi = 1/2Q = 1/260 = 0.0038$. The first model frequency of the cantilever was at $\omega = 2\pi \times 73881 \text{ rad/sec}$. For the one-mode model, the stiffness k was found to be 4.0 N/m .

A sinusoidal voltage at the resonant frequency ω of the cantilever was applied to the dither piezo attached to the cantilever base. The sample (silicon wafer) initially was sufficiently far from the cantilever so that it did not affect the cantilever motion. Once the cantilever reached its steady state ($\approx 1 \text{ ms}$), the sample was slowly moved towards the vibrating cantilever by extending the piezo on which the sample sits.

The motion of the cantilever tip at various values of the piezo extension was recorded using an HP 89410 vector signal analyzer. Time series plots of the steady-state behavior of the cantilever tip at different piezo positions are shown in Fig. 6. As established by the analysis we see that the cantilever tip is on a periodic orbit. The time period of the orbits determined from the plots is equal to $2\pi/\omega$. A spectrum analysis of the data shows that the orbits are nearly sinusoidal when the cantilever-sample separation is large. When the cantilever-sample separation is smaller, the cantilever motion deviates more from a sinusoidal behavior. However the net deflection of the nonsinusoidal motion is still at most one percent of the total motion. This agrees well with the

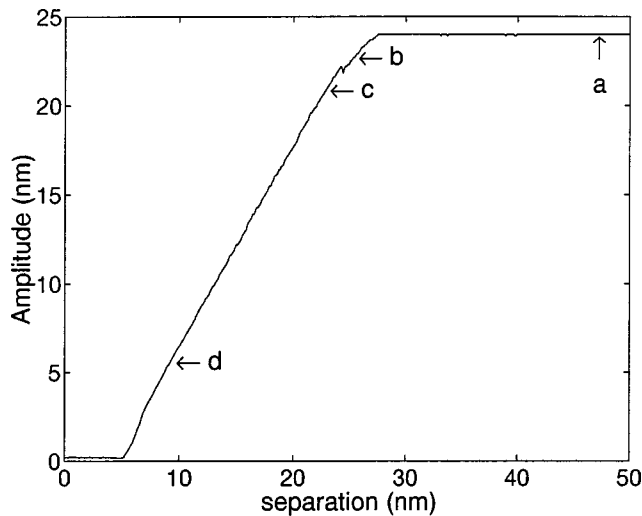


FIG. 7. This figure shows the plot of the amplitude of the first harmonic of the periodic oscillation of the cantilever tip with respect to the piezo extension that is a proportional measure of the cantilever-sample separation with an offset. In the region marked *a* the cantilever is not influenced by the sample at all. In the region indicated by *b* the cantilever is influenced only by the attractive regime of the tip-sample interaction, whereas in the region between *c* and *d* the tip is influenced primarily by the repulsive forces. The impact model is well suited to model the repulsive part of the tip-sample separation. As predicted by the analysis, the amplitude of the first harmonic varies linearly with the cantilever-sample separation in the region between *b* and *c*. Note that in the plot there is an offset between the amplitude and the separation. This is because there is an offset between the cantilever-sample separation and the piezo extension.

predictions made by assuming a impact model of the tip-sample interaction.

The piezo extension with respect to the voltage applied to the piezo scanner is linear in the relevant range (less than one-percent deviation). It needs to be stressed that the only quantifiable control on the cantilever-sample separation is through the piezo extension. There is no separate measure of the cantilever-sample separation. However, it can be assumed that there is a constant offset between piezo extension and the cantilever-sample separation. With this understanding the horizontal axis is labeled “separation” in Figs. 7 and 8.

The amplitude of the cantilever at various values of the separation are given in Fig. 7. The phase between the first harmonic of the periodic orbit and the forcing (denoted by ϕ) was also obtained experimentally (see Fig. 8). Systems like this that evolve to small impact velocities are known as grazing impact oscillators. It is evident from Fig. 7 that the amplitude of the first harmonic of cantilever’s oscillation varies linearly with respect to the separation, in the region between points *c* and *d* (see Fig. 7). Also, in Fig. 9, $\sin \phi$ is plotted against the separation. As can be seen, the experimental data shows that the plot is linear between the points *c* and *d*.

When the piezo extension is between the points marked *b* and *c* the cantilever tip barely (if at all) penetrates the repulsive region of the potential. The attractive region of the potential (see Fig. 2) has considerable influence on the cantilever motion. For values of the piezo extension in the region

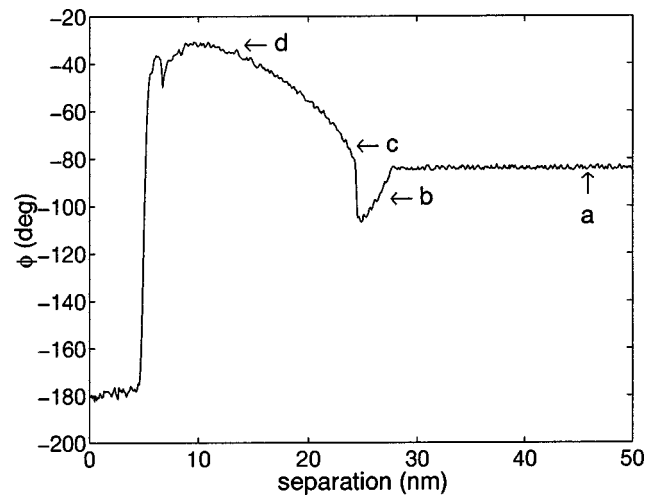


FIG. 8. The figure shows a plot of the phase between the first harmonic of the cantilever tip’s oscillation and the forcing. The various regions are explained in Fig. 7. It is difficult to extract any relationship between the phase and the cantilever-sample separation from this plot.

denoted by *a* the cantilever is not influenced by the sample and for values of the piezo extension more than that given by *d* the tip probably never leaves the moisture layer (see Ref. 16) present on the surface. The region between *b* and *c* can be explained by a model that includes the attractive part of the tip-sample interaction. Numerical modeling that includes a finite range attractive force in the tip-sample interaction does show this jump (see Ref. 8). For purposes of the analysis presented here, the appropriate region of the piezo extension is between the points *c* and *d* (the repulsive interaction regime). As is evident the plots of $\sin \phi$ and the amplitude are linear in this region, which agrees with the analytically obtained expressions in relations (19) and (20). Experiments

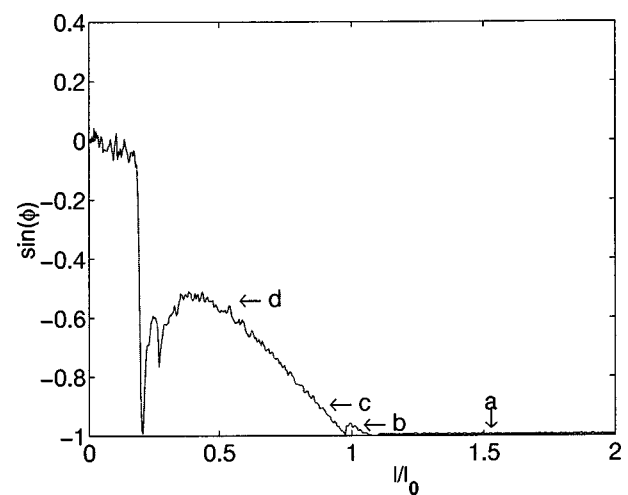


FIG. 9. This figure shows a plot of $\sin(\phi)$ versus scaled separation l/l_0 where l_0 is the amplitude of the free cantilever and ϕ is the phase between the first harmonic of the periodic oscillation of the cantilever tip and the forcing. The various regions are explained in Fig. 7. The linear relationship between $\sin(\phi)$ and cantilever-sample separation is evident in the region corresponding to the repulsive part of the tip-sample interaction (i.e., the region between *c* and *d*). This was predicted by the impact model.

conducted on a wide variety of samples show similar characteristics as illustrated in the experiment described in this paper.

The sample influences the amount of energy pumped into the system by the external forcing by changing the phase between the forcing and the orbit of the cantilever tip (here we are assuming with support from the analysis and experimental data that the periodic orbit can be approximated by a sinusoid and that the higher harmonics can be neglected). The sample also induces energy losses due to dissipative terms. When the energy lost to the sample (the dissipative energy loss) (estimated by using the method given in Ref. 17) is compared with the theoretically obtained result given by Eq. (17) we see that the energy lost due to impact cannot account for the net energy lost to the sample. The impact model predicts maximum energy losses ten times smaller than are observed experimentally. It is important to note that the same conclusion can be reached for *any* model where the tip-sample interaction is instantaneous. To see this, imagine a periodic orbit with any instantaneous interaction. Since the orbit is periodic, the tip will always have the same velocity \dot{p}_\perp before impact. Also the velocity \dot{p}_\perp after impact will be the same. Thus by defining the factor λ to be the ratio of these velocities the model is equivalent to the impact model on the periodic orbit and the relevant analysis carried out will apply.

Thus even though the fraction of the time the tip is interacting with the sample in a tapping AFM may be small, it is not negligible. This implies that any model that successfully predicts the energy losses will include finite interaction times. For hard samples, it is likely that the presence of the attractive forces (not included in the model analyzed in the paper) increase the interaction time. For soft samples like polymers, the repulsive forces are weak enough for the tip to spend significant time in the sample.

It should be noted that simulations have shown more refined models that include the attractive regime of the tip-sample interaction and account for the energy lost to the sample still preserve the linearity of amplitude and sine of phase predicted by the impact model. Analysis on experimental data over a wide variety of samples also confirms these conclusions.

V. CONCLUSIONS

In conclusion this work has shown that a very simple model, the impact model, provides remarkable insights into the tapping-mode dynamics. It predicts linearity of amplitude and the sine of the phase of the first harmonic of the cantilever-tip oscillation with respect to cantilever-sample separation. Experiments conducted on a wide variety of samples corroborate the results obtained. The linear relationships obtained can be used to devise new ways of imaging material. They also lend support to the assumption that the periodic orbit is nearly sinusoidal. This assumption has been used by many in the literature.

The impact model cannot account for the energy lost to the sample. One of the important insights obtained resulting from the analysis of this discrepancy is that any model that quantifies energy losses to the sample cannot ignore the interaction time between the sample and the cantilever tip.

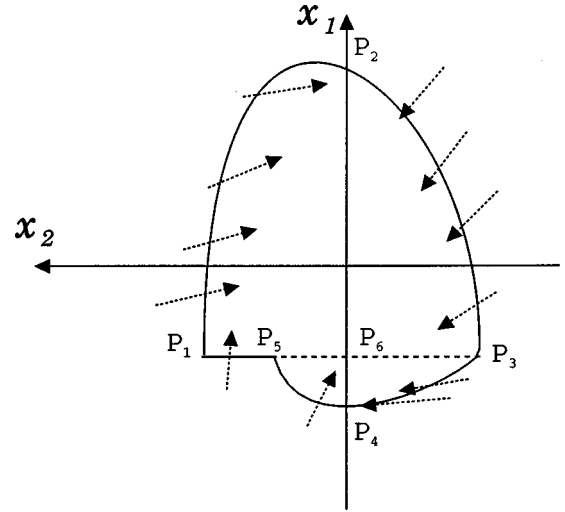


FIG. 10. Region D used in proving the existence of the periodic orbit.

This will aid the development of more refined models.

The existence of a periodic orbit is established with assumptions that are met by most tapping-mode operation conditions. Future research will develop models incorporating the insights obtained by this work.

ACKNOWLEDGMENTS

This work was supported by NSF under Grant Nos. ECS-9733802 and ECS-9410646.

APPENDIX

1. Results on existence of periodic orbits

In this section we will construct a positively invariant set D for the tapping-mode dynamics described by Eq. (3), where $h(x_1, x_2) = 0$ if $x_1 \geq -(l-d)$. We will first construct a set D_0 that is positively invariant under the dynamics of a damped oscillator described by Eq. (4).

Denote the total energy of the mass by $E = \frac{1}{2}\omega^2 x_1^2 + \frac{1}{2}x_2^2$. Let V be the modified energy function given by $V(x_1, x_2) := E + \xi\omega x_1 x_2$. Then,

$$(1 - \xi)E \leq V \leq (1 + \xi)E.$$

The derivative of $V(x)$ along a trajectory of Eq. (4) satisfies

$$\dot{V} \leq -2\xi\omega V(x) + 2\gamma\sqrt{V}.$$

Choose any $C \geq (\gamma/\xi\omega)^2$ and let $D_0(C) = \{x: V(x) \leq C\}$. Note that $D_0(C)$ defines a region enclosed by an ellipsoid. Also $D_0(C_i)$ lies entirely inside $D_0(C_j)$ if $C_i \leq C_j$. At any x on the boundary of D_0 , $V(x) = C$, and

$$\dot{V} \leq -2\sqrt{V}(\xi\omega\sqrt{V} - \gamma) \leq 0.$$

Thus on the boundary of $D_0(C)$, $x(t)$ is always moving in the direction of smaller V . Hence no trajectory of Eq. (4) can cross the boundary of D_0 outward.

Now we construct the set D that is positively invariant under the dynamics of Eq. (3), that is, we will construct a suitable set D which has the property that no solution starting

in D leaves D . Consider the region D enclosed by the closed curve $P_1P_2P_3P_4P_5P_1$ in Fig. 10. The arc $P_1P_2P_3$ is given by the set

$$\{(x_1, x_2): x_1 \geq -(l-d), \text{ and } V(x) = C\}.$$

Note that for x in the interior of the region enclosed by the curve $P_1P_2P_3P_4P_5P_1$, the dynamics are governed by Eq. (4). Therefore on the the curve $P_1P_2P_3$, the vector $f(x_1, x_2, t)$, where $f = f_1 + f_2g$, is directed as shown in Fig. 10.

The arc $P_3P_4P_5$ is given by the orbit of

$$\begin{pmatrix} \dot{x}_1 \\ \dot{x}_2 \end{pmatrix} = \begin{pmatrix} x_2 \\ -\omega^2 x_1 - 2\xi\omega x_2 - h(x_1, x_2) + \gamma \operatorname{sgn}(x_2) \end{pmatrix} =: \bar{f}(x), \quad (\text{A1})$$

which passes through the point P_3 . We make an assumption that the mass under the dynamics given by Eq. (A1) with initial condition P_3 will exit the sample at some point P_5 with a velocity whose magnitude is smaller than the magnitude of the velocity with which it entered the sample [that is $|x_2(P_5)| = \lambda|x_2(P_3)|$ with $0 < \lambda \leq 1$]. We will give justification for this assumption later.

For any point x on the arc $P_3P_4P_5$, at any time t , the angle made by the vector $f(x, t)$ with the positive x_1 axis is given by

$$\angle f = \tan^{-1} \left(\frac{-\omega^2 x_1 - 2\xi\omega x_2 - h(x_1, x_2)}{x_2} - \frac{\gamma \cos \omega t}{x_2} \right),$$

when $x_2 \neq 0$. Similarly, for any point x on the arc $P_3P_4P_5$, excluding the point P_4 , the angle made by the vector $\bar{f}(x)$ with the positive x_1 axis is given by

$$\angle \bar{f} = \tan^{-1} \left(\frac{-\omega^2 x_1 - 2\xi\omega x_2 - h(x_1, x_2)}{x_2} + \frac{\gamma}{|x_2|} \right).$$

As \tan^{-1} is a monotonically increasing function we have

$$\angle \bar{f}(x_1, x_2) \geq \angle f(x_1, x_2, t)$$

for all x on the arc $P_3P_4P_5$ [note that for the point P_4 , $\angle \bar{f}(P_4) = \angle f(P_4) = \pi/2$]. Thus no trajectory of Eq. (3) can leave the region D through the arc $P_3P_4P_5$.

The last part of the closed curve to be considered is the straight line P_1P_5 . Note that $V(P_1) = V(P_3) = C$. Also, for both P_3 and P_1 , the x_1 coordinate is equal to $-(l-d)$. Let $l' = -(l-d)$. Thus we have

$$\begin{aligned} & \frac{1}{2}\omega^2 l'^2 + \frac{1}{2}x_2^2(P_1) + \omega\xi l' x_2(P_1) \\ &= \frac{1}{2}\omega^2 l'^2 + \frac{1}{2}x_2^2(P_3) + \omega\xi l' x_2(P_3), \end{aligned}$$

which implies that

$$\frac{1}{2}[x_2^2(P_3) - x_2^2(P_1)] = -\xi\omega l'[x_2(P_3) - x_2(P_1)].$$

This implies that

$$x_2(P_3) = -x_2(P_1) - 2\xi\omega l'.$$

As $|x_2(P_5)| = \lambda|x_2(P_3)|$, it follows that

$$\begin{aligned} |x_2(P_1)| - |x_2(P_5)| &= |x_2(P_1)| - \lambda|x_2(P_3)| \\ &= (1-\lambda)|x_2(P_3)| - 2\xi\omega l' \\ &= (1-\lambda)|x_2(P_3)| + 2\xi\omega(l-d) > 0. \end{aligned}$$

It follows that the point P_5 is inbetween P_1 and P_6 as shown in Fig. 10. Finally, for all points $x = (x_1, x_2)$ on the line segment P_1P_5 , the value $x_1 < 0$ and $x_2 > 0$. This implies that no trajectory of Eq. (3) can leave D through P_1P_5 .

Thus no trajectory of Eq. (3) starting in the region D can leave D . Thus we conclude that the dynamics given by Eq. (3) has a T periodic solution lying entirely in D . Thus there exists a periodic solution with its period equal to T .

In arriving at the existence of a periodic orbit with period T we made the assumption that if the mass whose dynamics is governed by Eq. (A1) enters the sample's region of influence [the region $\{(x_1, x_2): x_1 \leq -(l-d)\}$], then it leaves the same region with a velocity whose magnitude is smaller than the magnitude of the velocity with which it entered it. For a typical tapping-mode operation, the tip-sample separation l is close to the resonant amplitude of the cantilever without the sample present. We denote the resonant amplitude by l_0 . Thus $|\omega^2 x_1| \approx \omega^2 l_0$ in the region of samples influence. Also, γ is given by $(\omega^2 l_0)/Q$ where $Q = 1/(2\xi)$. Typically the quality factor Q is above 100. It should also be noted that ξ is a small number and the attractive part of $h(x_1, x_2)$ is comparatively small in relation to the repulsive part. Thus it is expected that

$$-\omega^2 x_1 - 2\xi\omega x_2 - h(x_1, x_2) - \gamma > 0,$$

in the region of sample's influence. This means that the mass governed by Eq. (A1) will leave the region of samples influence. Also, the only way the mass can have a greater velocity when it leaves the region of sample's influence is if it has gained energy during the time it has spent there. The forcing γ is the only source by which the mass can gain energy. The variable d is small, thus the energy that the mass can gain due to the forcing while inside the sample is small with respect to the losses to the sample. In particular, the energy gained due to forcing is zero in the limit that the mass spends no time in the region of sample's influence. This justifies the assumptions made.

2. Results related to the impact model

The coefficients X , Y , and D are given by

$$\begin{aligned} X &= -\left(\frac{1}{\lambda} + 1\right) \frac{1}{\sqrt{1-\xi^2}} e^{-2\xi\pi} \sin(2\pi\sqrt{1-\xi^2}) \\ &= \frac{\lambda+1}{\lambda} \pi\xi^2 + O(\xi^3), \end{aligned} \quad (\text{A2})$$

$$\begin{aligned} Y &= \frac{1}{\lambda} e^{-4\xi\pi} + \left(-\frac{1}{\lambda} + 1\right) e^{-2\xi\pi} \cos(2\pi\sqrt{1-\xi^2}) \\ &\quad - \left(\frac{1}{\lambda} + 1\right) e^{-2\xi\pi} \frac{\xi}{\sqrt{1-\xi^2}} \sin(2\pi\sqrt{1-\xi^2}) \\ &= 2\pi\xi \left(\frac{\lambda+1}{\lambda}\right) + O(\xi^2), \end{aligned} \quad (\text{A3})$$

$$D = \frac{l}{l_0} Y. \quad (\text{A4})$$

The elements of the Jacobian matrix DP are given by

$$\begin{aligned} \frac{\partial P_1}{\partial \dot{p}_n} &= e^{-2\xi\pi} \left[-\lambda \cos 2\pi \sqrt{1-\xi^2} \right. \\ &\quad \left. + \frac{\lambda}{\sqrt{1-\xi^2}} \left(\frac{\ddot{p}_\downarrow}{\omega \dot{p}_\downarrow} + \xi \right) \sin 2\pi \sqrt{1-\xi^2} \right] \\ &= e^{-2\xi\pi} \left[-\lambda + \frac{l}{l_0} O(\xi) + O(\xi) \right] \\ \frac{\partial P_1}{\partial t_n} &= e^{-2\xi\pi} \left[-\lambda \cos 2\pi \sqrt{1-\xi^2} (-\lambda \ddot{p}_\downarrow - \ddot{p}_\uparrow) \right. \\ &\quad \left. - \frac{\lambda}{\sqrt{1-\xi^2}} \sin 2\pi \sqrt{1-\xi^2} \left(\frac{\ddot{p}_\downarrow (\ddot{p}_\uparrow + \xi \omega \dot{p}_\uparrow)}{\omega \dot{p}_\downarrow} \right. \right. \\ &\quad \left. \left. + \omega \dot{p}_\uparrow + \xi \ddot{p}_\uparrow \right) \right] \end{aligned}$$

$$\frac{\partial P_2}{\partial \dot{p}_n} = -e^{-2\xi\pi} \left(\frac{1}{\omega \dot{p}_\downarrow \sqrt{1-\xi^2}} \sin 2\pi \sqrt{1-\xi^2} \right),$$

$$= -e^{-2\xi\pi} \left(\frac{\xi}{2} + O(\xi^2) \right)$$

$$\frac{\partial P_2}{\partial t_n} = e^{-2\xi\pi} \left[-\lambda \cos 2\pi \sqrt{1-\xi^2} \right.$$

$$\left. + \frac{1}{\sqrt{1-\xi^2}} \left(\frac{\ddot{p}_\uparrow}{\omega \dot{p}_\downarrow} - \lambda \xi \right) \sin 2\pi \sqrt{1-\xi^2} \right]$$

$$= e^{-2\xi\pi} \left[-\lambda + \frac{l}{l_0} O(\xi) + O(\xi) \right],$$

where \ddot{p}_\downarrow and \dot{p}_\downarrow denote the acceleration and velocity of the mass on the periodic orbit before impact, whereas \ddot{p}_\uparrow and \dot{p}_\uparrow denote the acceleration and velocity of the mass on the periodic orbit after impact.

- ¹R. Wisendanger, *Scanning Probe Microscopy and Spectroscopy: Methods and Applications* (Cambridge University Press, Cambridge, 1994).
- ²G. Binnig, C. Quate, and C. Gerber, *Phys. Rev. Lett.* **56**, 930 (1986).
- ³B. Anczykowski, D. Kruger, K. L. Babcock, and H. Fuchs, *Ultramicroscopy* **66**, 251 (1996).
- ⁴M. Ashhab, M. V. Salapaka, M. Dahleh, and I. Mezic, in *Control of Chaos in Atomic Force Microscopes* (American Automatic Control Council, Albuquerque, NM, 1997).
- ⁵S. W. Shaw and P. J. Holmes, *J. Sound Vib.* **90**, 129 (1983).
- ⁶N. A. Burnham, A. J. Kulik, G. Gremaud, and G. A. D. Briggs, *Phys. Rev. Lett.* **74**, 5092 (1995).
- ⁷J. P. Cleveland, B. Anczykowski, A. E. Schmid, and V. B. Elings, *Appl. Phys. Lett.* **72**, 2613 (1998).
- ⁸A. Kuhle, A. H. Sorensen, and J. Bohr, *J. Appl. Phys.* **81**, 6562 (1997).
- ⁹D. Sarid, T. G. Ruskell, R. K. Workman, and C. Dong, *J. Vac.*

Sci. Technol. B **14**, 864 (1996).

- ¹⁰J. Tamayo and R. Garcia, *Langmuir* **12**, 4430 (1996).
- ¹¹R. G. Winkler, J. P. Spatz, S. Sheiko, M. Moller, P. Reuneker, and O. Marti, *Phys. Rev. B* **54**, 8908 (1996).
- ¹²M. Farkas, *Periodic Motions*, Applied Mathematical Sciences Vol. 104 (Springer-Verlag, New York, 1994).
- ¹³Q. Zhong, D. Inness, K. Kjoller, and V. Elings, *Surf. Sci.* **290**, L688 (1993).
- ¹⁴M. V. Salapaka, H. S. Bergh, J. Lai, A. Majumdar, and E. Mcfarland, *J. Appl. Phys.* **81**, 2480 (1997).
- ¹⁵D. A. Walters, J. P. Cleveland, N. H. Thomson, P. K. Hansma, M. A. Wendman, G. Gurley, and V. Elings, *Rev. Sci. Instrum.* **67**, 3583 (1996).
- ¹⁶S. Sounilhac, E. Barthel, and F. Creuzet, *J. Appl. Phys.* **85**, 222 (1999).
- ¹⁷J. P. Cleveland, Ph.D. thesis, University of California, Santa Barbara, 1995.